Autofocusing for Tuberculosis Detection using Fluorescence Microscopy

Otolorin A. Osibote, Ronald Dendere, Sriram Krishnan, Tania S. Douglas
MRC/UCT Medical Imaging Research Unit
University of Cape Town
South Africa

Abstract—**Automated microscopy in the context of tuberculosis (TB) screening aims to reduce the workload on technicians, especially in countries with a high burden of TB. Focusing is a key component of automated microscopy, and the selection of an appropriate autofocus algorithm is task-specific. We examined autofocusing algorithms for fluorescence microscopy of sputum smears for TB screening. Six focus measures, defined in the spatial domain, were applied to stacks of images of auramine-stained sputum smears. A maximum difference of 1.21 µm between manually focused and algorithm focused images was obtained for the best performing focus measures.**

Keywords-autofocus; focus measure; Mycobacterium tuberculosis; z-stack; curve-fitting

I. INTRODUCTION

Automation of microscopy for tuberculosis (TB) screening aims to speed up the screening process, to improve its sensitivity and to reduce its reliance on technicians. Algorithms for automated detection of *Mycobacterium tuberculosis* have been published for Ziehl-Neelsen (ZN) and for auramine stained sputum smears [1-3]. The recent availability of low-cost fluorescence microscopes [4] and the higher sensitivity of fluorescence microscopy of auramine-stained smears [5] motivate the consideration of automated fluorescence microscopy for TB detection.

Autofocusing is an important step in automated microscopy, as it determines the success of subsequent steps, namely image segmentation and the classification of segmented objects. The autofocus algorithm typically establishes a correspondence between the z-setting (the level of the microscope stage with respect to the objective) and the value of a focus measure, which evaluates the local image sharpness, attaining a maximum for the sharpest, or most in-focus, image [6,7]. Each image in a stack is evaluated to obtain a focus measure which is plotted against position in the stack. The optimum of the focus curve represents the best focus.

We evaluate spatial domain focus measures for stacks of images acquired using a fluorescence microscope.

II. METHODS

A. Image Acquisition

Image processing of fluorescence microscope images for identification of *Mycobacterium tuberculosis* has been reported for 25× objective magnification [1].

We used a Zeiss Axiovert 200M with a 20× objective lens at 0.75 numerical aperture for image acquisition. The accompanying Axiovision 4.7 software allows control of the motorized z-drive in exact steps, synchronizing it with image acquisition. To acquire a z-stack of a field, the position of maximum focus as judged by a human observer was recorded, the start and end points of the stack were defined on either side of the focal position, and images were captured at 1.2 µm z-increments. The images were captured using an AxioCamHR camera and stored with 1292 × 1014 pixel resolution in 8-bit JPEG format.

Two adjacent z-stacks of 24 images each were captured from each of two auramine-stained sputum smear slides, confirmed positive for TB. Focus measure curves were calculated and analyzed to determine whether the global maximum corresponds to the best focused image as judged by a human expert. In addition, curves fitted to a reduced number of image focus measure values were examined in order to determine if speeding up the focusing process in this manner yielded acceptable results.

B. Focus Measures

No generally applicable autofocusing solution has been proposed for microscopy [8]; we therefore examined six focus measures which have been effective for a wide range of biological and biomedical applications.

The sum-modified-Laplacian (SML) calculates the sums of the absolute values of the convolution of an image with modified Laplacian operators [9]:

$$\nabla^2{}_M I = \left|\frac{\partial^2 I}{\partial i^2}\right| + \left|\frac{\partial^2 I}{\partial j^2}\right|$$

where I is the image intensity at point (i, j).

The normalized variance (NV) compensates for the differences in average image intensity among different images by normalizing the gray level variance with the mean intensity μ [8,10]:

Funding was provided by the NIH/NIAID (R21AI067659-02)

$$F_{NV} = \frac{1}{M \times N \times \mu} \sum_{i=1}^{M} \sum_{j=1}^{N} [I(i,j) - \mu]^2$$

where M and N are the height and width of the image respectively.

The energy of the Laplacian of the image (EOL) uses the Laplacian operator to determine high spatial frequencies associated with sharp borders in the image [10]:

$$F_{EOL} = \sum_{i}^{M} \sum_{j}^{N} (I_{ii} + I_{jj})^2$$

I_{ii} and I_{jj} are second derivatives of I with respect to *i* and *j*.

Tenenbaum's algorithm (Tenengrad) is a gradient magnitude maximization method that measures the sum of the squared responses of the horizontal and vertical Sobel masks [10]:

$$F_{Tenengrad} = \sum_{i=2}^{M} \sum_{j=2}^{N} [\nabla I(i,j)]^2$$

where $\nabla I(i,j)$ is the Sobel gradient magnitude

The Brenner gradient (BG) measures the difference between a pixel and a neighbour [11]:

$$F_{Brenner} = \sum_{i=1}^{M} \sum_{j=1}^{N} [I(i,j) - I(i+m,j)]^2$$

where $m = 2$ i.e. a neighbour is two pixels away.

Vollath's F_4 is based on the autocorrelation function [12].

$$F_{vollath} = \sum_{i=1}^{M-1} \sum_{j=1}^{N} I(i,j) \times I(i+1,j) - \sum_{i=1}^{M-2} \sum_{j=1}^{N} I(i,j) \times I(i+2,j)$$

C. Curve Fitting

Reducing the number of images used to bring the sample into focus will speed up the autofocusing process. To this end, a curve may be fitted to the focus measures of a few images selected at different positions along the z-axis [11]. The peak of the fitted curve is an estimate of the focal position. The distribution of the focus measures is expected to be Gaussian and therefore a Gaussian function can be fitted to the focus measures; a quadratic function fitted to the logarithm of the data will produce a similar result [13]. Fitting a polynomial of order *n* requires at least *n+1* images; we therefore need 3 images to find the position of optimal focus. The images have to be located on either side of the focal position, which requires a rough estimate of the focal position. Curves were fitted to two images captured one step on either side of the focal position and a third at two steps away on any side.

III. Results

A comparison of typical curves for stacks of 24 images and for only three images, with a fitted curve, is shown in Figure 1. The focus measure values were normalized by their maximum and the fitted logarithms of the values obtained from three images were normalized by their maximum for positive values and by their minimum for negative values. Table I gives the magnitude of the difference between the focal position as determined by an expert (F_A) and the estimated focal position (F_E) from the plotted curve, as well as the processing times (using MATLAB) – these would be system-dependent, and are given to allow comparison across methods.

IV. Discussion

All six focus measures performed well, producing curves in which the average position of the peaks is within a step (1.2 µm) of the focal position as determined by an expert. Tenegrad, Brenner gradient, Vollath's F_4 produced focal positions closest to those of a human observer, while Tenengrad had the slowest execution time. With curve fitting, good focal position estimates were obtained when two images captured one step on either side of the focal position and the third image at two steps on any side, were used; capturing these images further from the focal position increased the deviation from F_A. In practice, such curve fitting would reduce autofocus time after the first field in a slide has been focused using a complete image stack, as the position of optimal focus for a field may be regarded as an estimate of that of an adjacent field. The differences in F_E (calculated using the full image stack) for adjacent fields were 0.5 µm and 0.6 µm, respectively, for the two slides we used. This difference in adjacent focal positions is less than a step size, while the maximum difference between expert and estimated focal positions for the best performing focus measures is close to a step size. Thus selection of images of a new field for curve fitting around the focal position of the previous field in a sequence on the same slide would allow acceptable estimation of the new focal position. Figure 2 shows an in-focus fluorescence image.

In real-time autofocusing applications, the time taken for the mechanical motion of the objective with respect to the sample to view different fields is the greatest source of delay [14]. The execution times presented therefore do not reflect those of a practical autofocusing implementation.

V. Conclusion

The Tenengrad, Brenner gradient and Vollath's F_4 focus measures hold promise for autofocusing in fluorescence microscopy for TB screening. At 20× objective magnification, the focal position of a field may be used as an estimate of that of an adjacent field, in order to reduce focusing time.

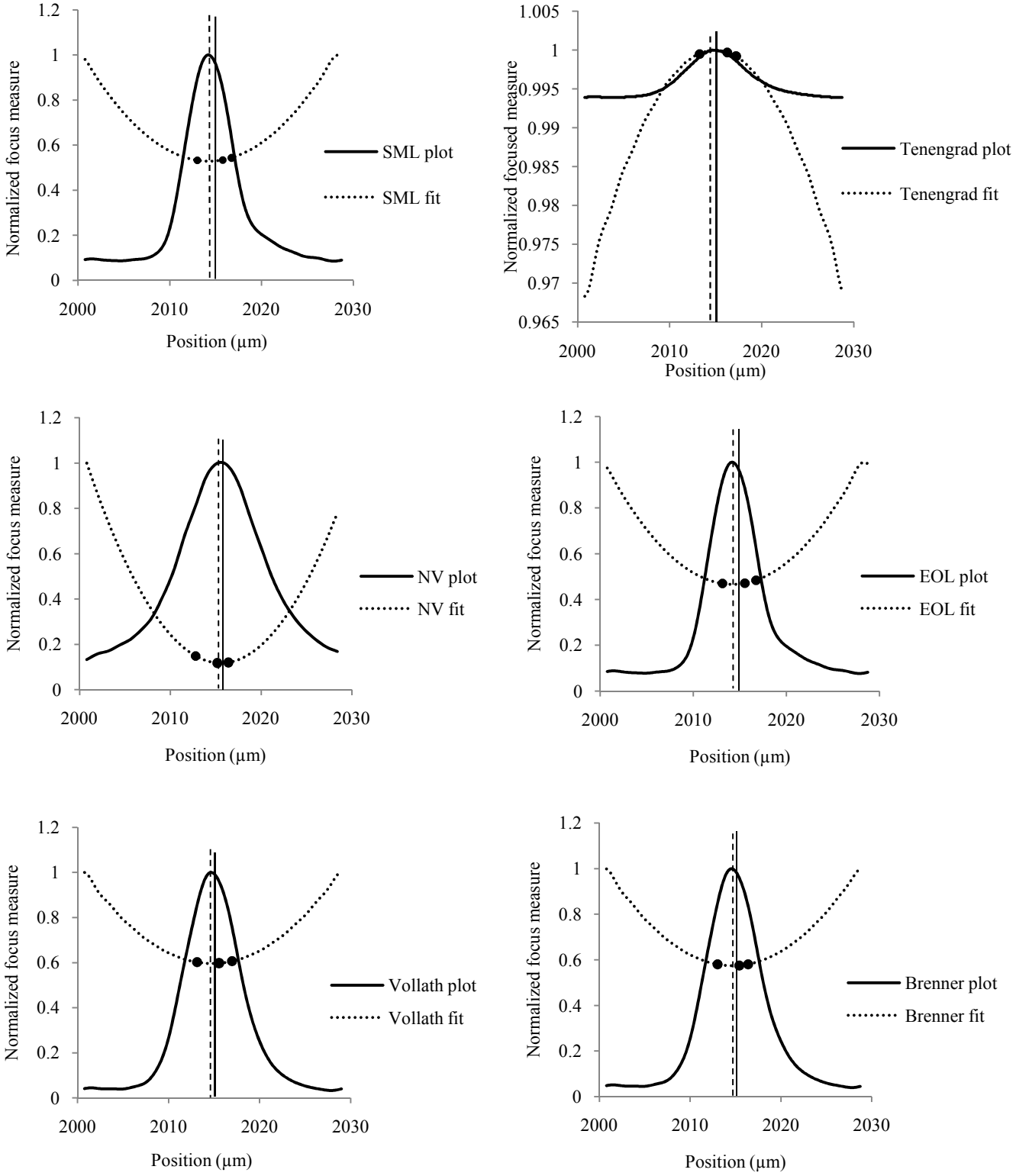

Figure. 1. Focus functions extracted from the full stack of 24 images (solid curve) and from only 3 images (dashed curve – logarithm of the focus measures). The dark circles represent the position at which the three images used for fitting were captured. The vertical dashed line represents the position of the optimum of the 24 z-stack values, and the vertical solid line, the optimum of the fitted curve. The difference in orientation of the 3-image curves is due to the difference in sign of the logarithms of corresponding focus function values.

TABLE I. COMPARISON OF FOCUS MEASURE PERFORMANCE; F_A=FOCAL POSITION SELECTED BY MICROSCOPE USER AND F_E=ESTIMATED FOCAL POSITION

Focus function	Original Curve (24 images)				Fitted Curve (3 images)			
		$\|\|F_A - F_E\|\|$ (μm)				$\|\|F_A - F_E\|\|$ (μm)		
	Time (s)	Minimum	Maximum	Mean	Time (s)	Minimum	Maximum	Mean
SML	5.72	0.51	1.45	0.91	0.75	0.39	1.25	0.73
NV	4.48	0.45	1.39	0.97	0.60	0.69	2.35	1.29
EOL	7.28	0.51	1.45	0.87	0.93	0.51	1.25	0.77
TENENGRAD	12.12	0.09	1.21	0.81	1.65	0.05	0.85	0.37
BG	4.61	0.15	1.21	0.79	0.64	0.05	0.85	0.35
VOLLATH'S F_4	4.98	0.03	1.21	0.72	0.77	0.03	0.85	0.31

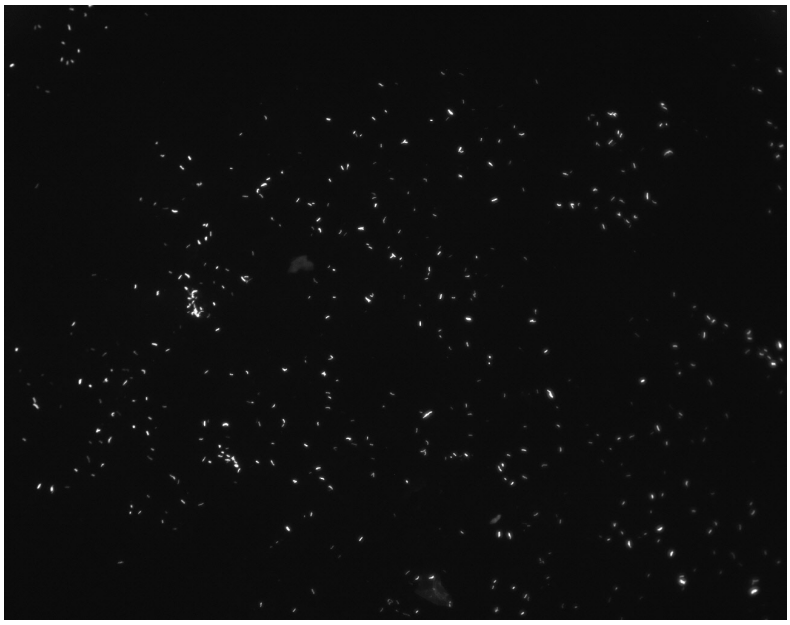

Figure 2. Example of an in-focus image of an auramine-stained sputum smear under a fluorescence microscope.

REFERENCES

[1] M. G. Forero, G Cristobal, M. Desco, "Automatic identification of Mycobacterium tuberculosis by Gaussian mixture models," J. Microscopy, vol. 223, pp 120-132, 2006.

[2] K. Veropoulos, G. Learmonth, C. Campbell, B. Knight, J. Simpson, "Automated identification of tubercle bacilli in sputum - a preliminary investigation," Analytical and Quantitative Cytology and Histology vol. 21, pp 277-281, 1999.

[3] R. Khutlang, S. Krishnan, A. Whitelaw, T. S. Douglas, "Automated detection of tuberculosis in Ziehl-Neelsen stained sputum smears using two one-class classifiers," J. Microscopy, 2010, vol. 237, pp 96-102, 2010.

[4] T. Hanscheid, "The future looks bright: low-cost fluorescent microscopes for detection of Mycobacterium tuberculosis and Coccidiae," Transactions of the Royal Society of Tropical Medicine and Hygiene, vol. 102, pp 520-521, 2008.

[5] K. R. Steingart, M. Henry, V. Ng, P. C. Hopewell, A. Ramsay, J. Cunningham et al., "Flourescence versus vonventional sputum smear microscopy for tuberculosis: A systematic review," Lancet Infectious Diseases, vol. 9, pp 570-81, 2006.

[6] J. He, R. Zhou, Z. Hong, "Modified fast climbing search autofocus algorithm with adaptive step size searching technique for digital camera," IEEE Trans. Cons. Electronics, vol. 49,pp 257-262, 2003.

[7] S. Malik and T. Choi, "A novel algorithm for estimation of depth map using image focus for 3D shape recovery in the presence of noise," Pattern Recognition, vol. 41,pp 2200-2225, 2008.

[8] F. Groen, I.T. Young, G. Ligntart, "A comparison of different focus functions for use in autofocus algorithms," Cytometry, vol. 6, pp81-91, 1985.

[9] S. K. Nayar and Y. Nakagawa, "Shape from Focus," IEEE Trans. PAMI, vol. 16, pp 824-831, 1994.

[10] W. Huang and Z. Jing, "Evaluation of focus measures in multi-focus image fusion," Patt. Recog. Lett., vol. 28, pp 493-500, 2007.

[11] S. Yazdanfar, K. B. Kenny, K. Tasimi, A. D. Corwin, E. L. Dixon, R. J. Filkins RJ, "Simple and Robust Image-based Autofocusing for Digital Microscopy", Optics Express, vol. 16,pp 8670-8677, 2008.

[12] D. Vollath, "The influence of the scene parameters and of noise on the behaviour of automatic focusing algorithms," J. Microscopy, vol. 151, pp 133-146, 1988.

[13] J. O. Smith (2008, October). Spectral Audio Signal Processing [Online]. Available: http://www.ccrma.stanford.edu/~jos/sasp

[14] M. Subbarao and J. K. Tyan, "Selecting the optimal focus measure for autofocusing and depth-from-focus," IEEE Trans.PAMI, vol. 20, pp864-70, 1998.